**J. Marty, L. Castillon,**
**J.-C. Boniface,**
(Onera)
**S. Burguburu**
(Snecma)
**A. Godard**
(Ecole Centrale de Lyon)

E-mail: julien.marty@onera.fr

# Numerical and Experimental Investigations of Flow Control in Axial Compressors

The increase of the thrust-to-weight ratio of modern gas-turbine engines results in higher loads and a reduced number of blades and stages for the compressor. The designer must ensure the acceptable performance of each compressor stage (efficiency and stable operating range) and control the rising risk of blade boundary layer separation. This can be obtained using passive or active control devices which act on the behavior of the tip leakage flows or the endwall corner stall when the operating point gets closer to the stall or surge limit (compressor). This study focuses on casing treatments, with axisymmetrical and non-axisymmetrical slots, on injection or recirculating grooves, which are efficient approaches to extend the stable operating range, especially by increasing the stall margin of a compressor system while the efficiency penalty must remain as small as possible. The hub corner stall is controlled by aspirated compressor and vortex generators.

## Introduction

The current trend in gas-turbine engine design is to increase the thrust-to-weight ratio. This leads to a compressor design with higher aerodynamic loads and a reduced number of blades and stages. The pressure rise per stage and the efficiency must be increased. Nevertheless, the increased blade loading tends to decrease the stall margin and therefore the stable operating range of compressors. Many passive or active control devices are used to increase the efficiency and/or the stable operating range of the compression system without any penalty on other performance parameters.

The aerodynamic stability of a compressor is limited by the behavior of the tip leakage flows or the hub corner stall when the operating point gets closer to the stall or surge limit. One approach to increase the compressor stability consists in the use of casing treatments, such as circumferential, non-axisymmetrical or axial skewed grooves to control the tip flow. Some authors focus on the extension of the operating range using casing treatments delaying stall limit ([13][16][43]). Nevertheless, the casing treatment can induce additional losses at peak efficiency condition. According to earlier research, the stall margin increase varies between 6 and 10% and the variation of efficiency is about $\pm 0.5\%$ compared to a smooth casing configuration. The efficiency of the casing treatment depends on the slot location. Rabe and Hah [40] show that grooves close to the trailing edge seemed ineffective. The influence of the groove position was also studied by Perrot et al. [39]. The configuration consists of five circumferential grooves. They reported that for this configuration only the first groove has a beneficial effect at near stall operating conditions and increases stall margin, while the second one improves the pressure ratio and efficiency. This influence of the groove position was also observed by Legras et al. [29].

Another approach to control the flow near the rotor blade tip is based on the injection of high momentum fluid and/or bleed of low momentum fluid. The combination of injection and bleed leads to recirculating flow: the compressor static pressure rise induces a recirculation of high pressure flow from the rear to the front of a rotor. This can be achieved by either a single bridge, which creates a natural flow from TE to LE, or experimentally by two separate devices: one for the suction and another for the blowing. Hathaway [23] investigates the influence of the injection, bleed and recirculation applications on the operating range. The latter can be increased up to 60% with bleed near the trailing edge, 38% with fluid injection upstream of the lower momentum region and 64% with recirculating flow where the massflow rate reaches 1.9% of the choke massflow rate. Suder et al. [48] found that the tip injection increases stability. The stalling flow coefficient can be reduced by 6% with an injected massflow which is equal to 2% of the annulus flow. The extension of the stable operating range was also investigated by Weigl and Spakovsky ([44][45][50]).

The hub or casing corner stall is also a source of important losses and can be the cause of stall or surge. The injection and bleed techniques can be used to control this kind of flow. Several authors found the beneficial effect of the boundary layer suction at the endwall and/or at the blade wall ([12][17][37][41]). Another approach is based on the vortex generators (VG). Their induced vortices mix high and low momentum flow near the wall, allowing the boundary layer to over-

come a strong adverse pressure gradient. Chima [11], Hergt et al. [25], Ortmanns et al. [36] applied VG to control the secondary flows, especially the hub or casing corner stall. In aircraft applications, they are usually employed to delay stall.

This paper does not deal with the technology involved in the control device but focuses only on the methodology to simulate the aerodynamic effect of the control device. It is also important to keep in mind that the purpose of this paper is not to give a deep and exhaustive physical analysis of turbomachinery flows subjected to control methods, nor to give advice concerning the best way to perform an efficient flow control. That would be a difficult challenge far beyond the scope of this paper. Our goal here is more to give a synthetic overview of handy numerical methods developed at Onera, which can be used by aero-engine designers in an industrial context in order to investigate control techniques and optimize control devices. Ongoing numerical activities carried out at the Applied Aerodynamics Department of Onera for passive or active flow control devices applied in turbomachinery are presented below. The methodology developed for flow control within a CFD analysis is described first. Investigations on flow control, especially on the compressor side, are reviewed: (i) tip leakage flow control considering axisymmetrical and non-axisymmetrical casing treatments, (ii) tip flow control with the help of suction, blowing or recirculating grooves, (iii) secondary flow and boundary layer flow control by using vortex generators or aspiration devices.

## Methodology

The elsA solver, developed at Onera since 1997, is a multi-application aerodynamic code based on a cell-centered finite-volume discretization in structured meshes. From the solution of the compressible, three-dimensional Reynolds-averaged Navier-Stokes equations (RANS), the elsA solver has been developed to handle a wide range of aerospace configurations such as aircrafts, space launchers, missiles, helicopters and turbomachines ([7][8]). A large variety of turbulence models, ranging from algebraic to non-Boussinesq modeling, have been implemented.

The centered space-discretization scheme of Jameson or the upwind Roe-MUSCL solver are some of the classical second-order space-discretization schemes used for turbomachinery applications. A second-order accurate Roe scheme is used for the transport equations of turbulence models. Several time-integration schemes can be considered to perform steady and unsteady computations. Explicit or implicit schemes, such as a pseudo-time approach (Dual Time Stepping) or the Gear Method, are available. Time integration can be solved either by an implicit residual smoothing phase with a 4-step Runge-Kutta technique, or by an implicit LU scalar relaxation phase associated with a backward Euler scheme. In steady flow assumption, standard convergence acceleration techniques, such as local time stepping and multi-grid methods improve the convergence rate, thus reducing the global CPU time.

Suitable boundary conditions for turbomachinery configurations have also been implemented, in order to compute steady flows: coincident and non-coincident matching conditions have been developed for the treatment of the periodicity condition and a steady multi-stage condition using pitch-averaging for the treatment of the rotor-stator interface. Physical boundary conditions include different types of inlet, outlet and wall conditions.

For structured-grid flow solvers, a major issue is the difficulty in generating meshes around complex configurations. One way to alleviate this problem is to use the Chimera technique ([3][4]), which has been widely developed in the elsA software ([5][26]) and applied to turbomachinery configurations [9]. This overset grid approach operates as a matching condition between blocks that overlap and can be generated independently around each body. Any grid can overlap with an arbitrary number of other grids, which may overlap themselves. The RANS equations are solved on each grid system and transfers are then performed between overlapping grids by interpolation of the conservative and turbulent variables, first at overlapping boundaries and then around blanked mesh-cells lying inside solid bodies. A cell search procedure is performed using an alternating digital tree research algorithm (ADT) [6] which determines the donor cell and the interpolation coefficient for a given target cell. Multiply-defined walls are treated using the Schwarz algorithm [42] for interpolation coefficient calculations. Several hole-cutting techniques have been developed, including the Object X-Ray technique, originally developed by Meakin [31].

A major advantage of the Chimera method is that it significantly simplifies the process of mesh generation by using overlapping grids. Different parts of the grid can therefore be generated independently: for example, the blade channel can be constructed on one side with a family of coincident structured blocks, while and a second family of structured coincident domains can be generated on another side (eventually with a different grid generator) to mesh a technological component or a control device. This approach is also very well suited for parametric studies on the characteristics of the technological components or the control actuator, since there is no need the re-mesh the entire configuration. For example, while investigating the impact of the size or of the position of a technological effect on the flow field, it is only necessary to modify the grids associated with this geometrical component.

## Tip Blade Flow Control

### Axisymmetric Casing Treatment

The casing treatment consists of slots or grooves within the rotor casing and is used to extend the surge margin of the compressor ([22] [24]). Two sets of casing treatment are studied. The first one, called "HCT", is based on the work of Müller et al. [34] and the second one "SCT" is based on the work of Legras et al. [27]. The location of the first slot, the height, width and spacing of the slots are normalized by the axial chord $C_{ax}$ at the blade tip. The HCT and SCT normalized values are summed up in table 1. The main discrepancy between the two casing treatments concerns the slot height h and the location of the leading edge of the first slot $X_{LE}$. The height, width and spacing of the slots, the leading edge of the first slot and the slot number are schematized in figure 1.

The considered test-case is the first rotor of the 3.5-stage research compressor CREATE. This compressor is representative of median or rear stages of a modern, highly loaded multi-stage compressor. For the CREATE facility, the number of blades of each rotor and stator is a multiple of 16. The rotational speed is 11500 rpm and the design massflow is 12.7 kg/s. Experimental data have been obtained through detailed instrumentation of the compressor, using both pneumatic measurements and laser Doppler anemometry techniques on several measurement planes. The measurements are performed in the circu-

| Normalized values | Location of the slot leading edge | Width | Height | Spacing | Slot number |
|---|---|---|---|---|---|
| HCT | LE+15.25%$C_{ax}$ | 0.0976$C_{ax}$ | 0.2927$C_{ax}$ | 0.04878$C_{ax}$ | 6 |
| SCT | LE-5%$C_{ax}$ | 0.109$C_{ax}$ | 0.0763$C_{ax}$ | 0.0545$C_{ax}$ | 6 |

Table 1: Casing treatment characteristics, extracted from [34] and [27]. LE and $C_{ax}$ mean respectively rotor leading edge and rotor axial chord length

mferential direction at different constant radius locations downstream of each row. Since the spatial periodicity of the compressor is 22.5°, the azimuth measurements allow aerodynamic phenomena interacting over a complete spatial period to be represented. A detailed description of the compressor is provided by Touyeras and Villain [49] and by Arnaud et al. ([1][2]).

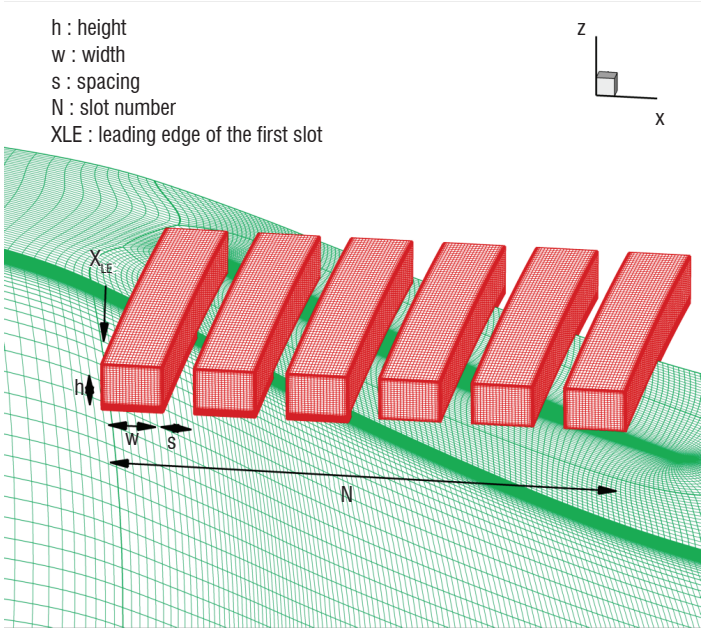


Figure 1 - Schematic view of casing treatment

Since the casing treatment is axisymmetric and the numerical domain is an isolated row, steady simulations are performed using the Chimera approach. A fully turbulent flow assumption is made and the Spalart-Allmaras turbulence model has been considered [46]. The computational domain consists of one rotor blade channel and six casing treatment slots. The mesh is composed of $5.5.10^6$ points. The values of $y^+$ at the blade wall are lower than 1 in the entire domain.

The radial velocity field is depicted in figure 2 at three given azimuths and one selected radius. The operating point is the nominal point for the three simulations. The tip leakage vortex can be identified by the alternation of negative (blue) and positive (red) radial velocity on the constant radius plane. The casing treatments strongly modify the flow and vortex development in the vicinity of the blade tip. Due to the grooves, the expansion of the tip leakage vortex is limited in the direction perpendicular to the blade chord. For both simulations with slots, the impingement point of the tip leakage vortex on the adjacent blade is located downstream of the reference point. This modification of the tip leakage vortex trajectory is one reason for the stall margin increase. It should be noticed that all casing treatments induce a slight reduction of the isentropic efficiency. The main discrepancy between the two slot configurations concerns the flow topology within the casing treatments. A large part of the HCT is useless as the radial velocity is close to zero and the two downstream grooves have a small influence as the casing treatment acts significantly in the vicinity of the tip leakage vortex appearance. Thus, the position and height of the casing treatments are important parameters for the slot design. As a general rule, the design of the casing treatment depends strongly on the configuration and should be designed simultaneously with the rotor blade tip.

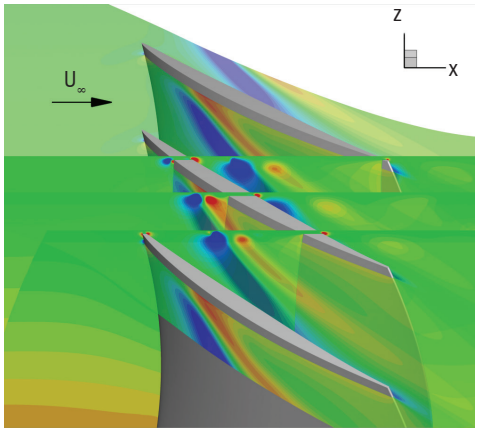


(a) Without casing treatment

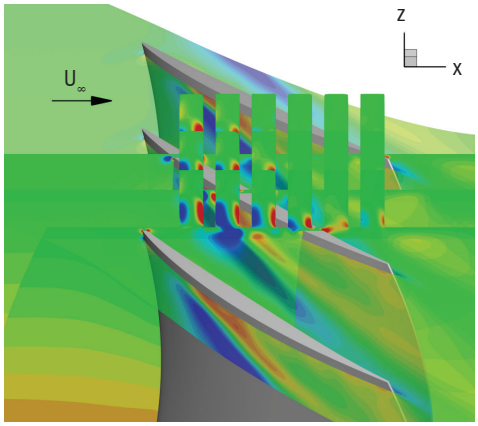


(b) With casing treatment (HCT)

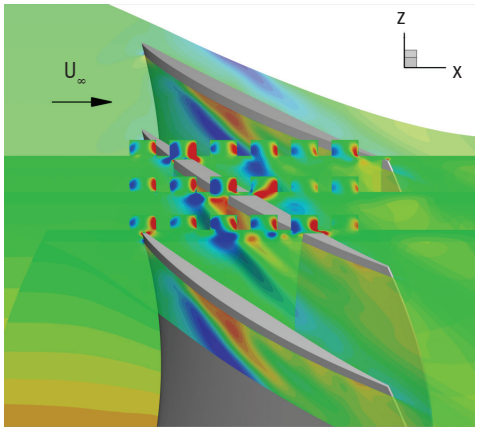


(c) With casing treatment (SCT)

Figure 2 - Radial velocity field. Negative and positive values are respectively in blue and red

## Non-axisymmetric Casing Treatment

Many experimental and numerical works achieved in the past have shown the interest of using casing treatments on compressor configurations, in order to extend stall margins. Investigations on the impact of non-circumferential casing treatments have been performed at Onera ([10][28]). An unsteady Chimera approach combined with a phase-lag technique has been developed in the elsA code to simulate non-circumferential casing treatments and the unsteady interactions between rotors and slots. The configuration is the experimental transonic rotor tested at the School of Jet Propulsion, Beijing University of Aeronautics and Astronautics (BUAA), composed of 17 rotor blades with 9 slots per blade passage ([30][35]) as represented in figure 3. A view of the grid is presented in figure 4 (left), the two families of blocks (channel and casing treatment) overlap in the meridian plane in order to ensure continuity of the flow field at their interface. The computational domain, composed of one rotor blade channel and one casing treatment slot, is meshed with a 13 block structured grid including $3.10^6$ points. The values of $y^+$ at the blade wall range from 1 to 2.

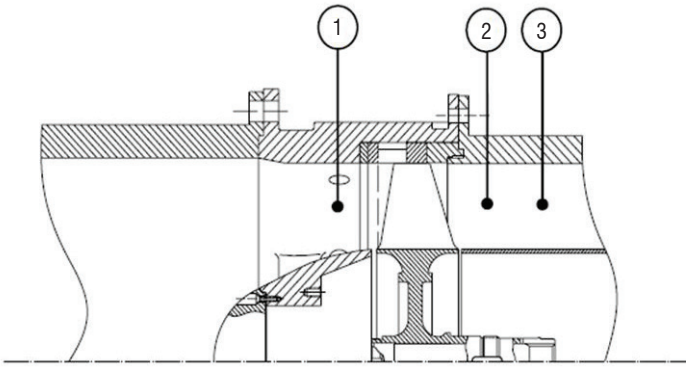


1 - Inlet plane: one total pressure comb
2 - Outlet plane I: one fast response pressure probe, monitoring the onset of rotating stall
3 - Outlet plane II: two total pressure combs

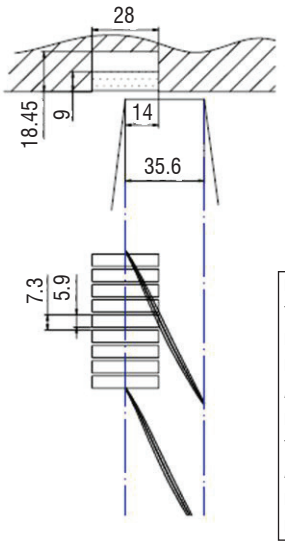


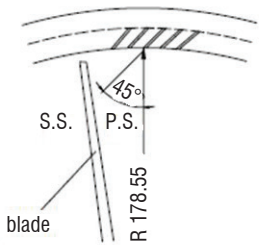


| | |
|---|---|
| Blade number | 17 |
| Tip diameter | 355.8 mm |
| Design speed | 22 000 rpm |
| Hub-to-tip ratio | 0.565 |
| Aspect ratio | 0.956 |
| Mass flow at design point | 13.4 kg/sec |
| Total pressure ratio at design point | 1.6 (stage) |
| Adiabatic efficiency at design point | 0.88 (stage) |
| Relative Mach number of inflow at rotor up | 1.404 |
| Nominal tip clearence at 100% speed | 0.25 mm |

Figure 3 - Cross-section view of the test section (top) and sketch of the slot type casing treatment (Lin et al. [30])

The Chimera method developed enables the capturing of the unsteady flow migrations between the slots and the rotor channel, as can be seen in figure 4 (right), which represents a snapshot of the radial velocity distribution near the casing. Two zones can be distinguished: the zones of positive radial velocity in the downstream part of the slot, corresponding to the flow entering into the casing treatment, and the zones of negative radial velocity, where the flow is reinjected into the rotor channel.

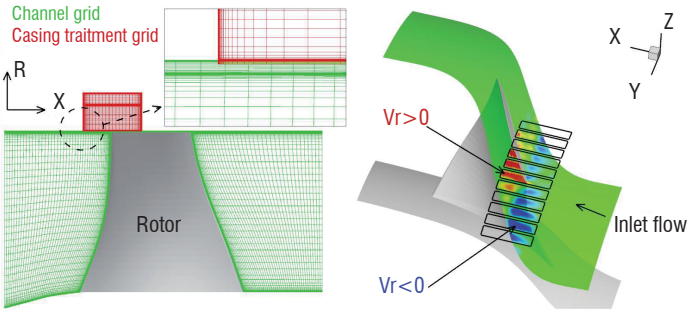


Figure 4 - Left: BUAA overset grids. Right: snapshot of the radial velocity distribution near the casing

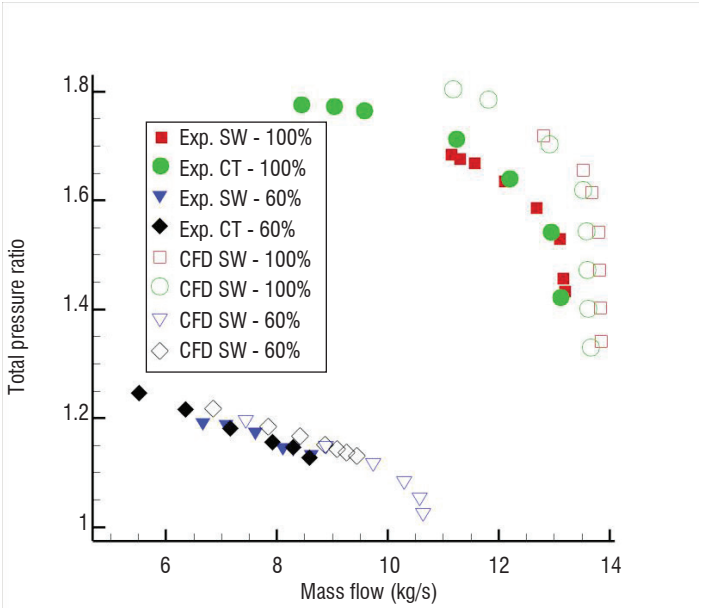


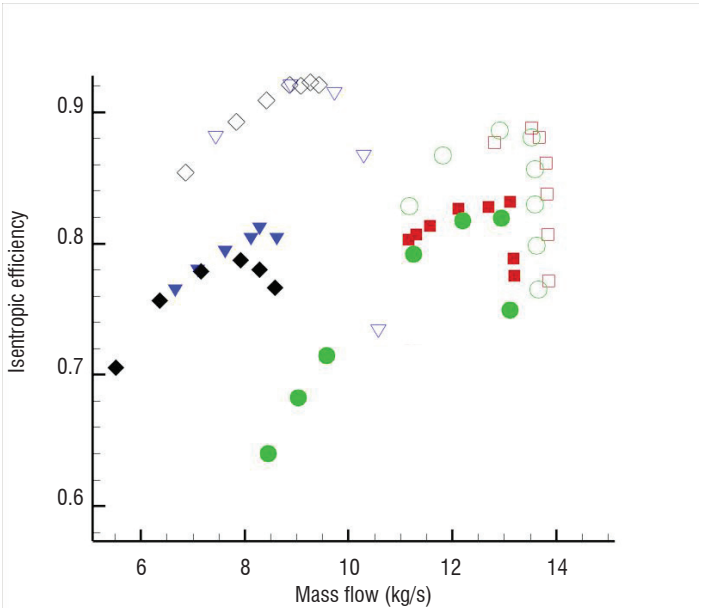


Figure 5 - Experimental and computed compressor maps

The experimental and computed compressor maps are presented in figure 5; the pressure ratio and the isentropic efficiency are plotted as a function of the massflow. Smooth wall calculations (SW), performed by removing the computational grid of the slots are compared to

| Configuration | CB (Casing Blowing) | RF1(Recirculating flow configuration 1) | RF2(Recirculating flow configuration 2) |
|---|---|---|---|
| LE of the blowing groove | LE – 9.5%$C_{ax}$ | LE + 30 %$C_{ax}$ | LE – 9.5%$C_{ax}$ |
| Width of the blowing groove | 3.8%$C_{ax}$ | 10 %$C_{ax}$ | 3.8%$C_{ax}$ |
| Blowing massflow | 1% nominal massflow | 1.9% choke massflow | 1% nominal massflow |
| Angle between the blowing groove axis and the rotation axis 'x', in (x,R) plane | 14° | 30° | 15° |
| LE of the suction groove | – | TE + 5 %$C_{ax}$ | TE + 5 %$C_{ax}$ |
| Width of the suction groove | – | 10 %$C_{ax}$ | 10 %$C_{ax}$ |
| Suction massflow | – | 1.9% choke massflow | 1% nominal massflow |
| Angle between the suction groove axis and the rotation axis 'x', in (x,R) plane | – | -30° | -30° |

Table 2 - Characteristics of active flow control devices. LE and $C_{ax}$ mean respectively rotor leading edge and rotor axial chord length

casing treatment (CT) configurations, for two rotation speeds (60% and 100% of the rotor design wheel speed). Both experiments and CFD analysis show that the slots enable to increase the stall margin of the rotor, even if the extension improvement is underestimated in CFD. At nominal rotation speed, the casing treatment also induces a slight penalty on the peak efficiency and on the chocking massflow rate. The underestimation of the stall margin increase can be explained by the fact that the method is based on a phase-lag assumption, which assumes that the flow is periodic, this hypothesis being far from true near stall. Nevertheless, the key point is that a significant impact of the casing treatment is observed in the calculation. Results obtained with the experimental BUAA configuration show that the method correctly reproduces the effect of the stall margin increase induced by the casing treatments, even if the stall margin increase is underestimated in the CFD analysis.

## Tip Blade Suction and Blowing, Recirculating flow

Casing treatments are passive control devices, since no external energy source is required. Active control devices have been also investigated, as supplying momentum in the main flow path using an axisymmetric groove. The injected massflow can be provided by an aspiration slot located downstream. In this case, a recirculating flow occurs (figure 6). The current study focuses on three configurations. The main characteristics of these configurations are reported in table 2. The configuration RF1 is based on the work of Hathaway [23].

The experimental facility is again the first rotor of the research compressor CREATE, which has been described in the previous section. The blowing and suction grooves are included in the simulation using the Chimera method. The computational domain consists of one rotor blade channel and the active control grooves. The mesh density is 4.5.106 points for the CB configuration and 4.7.106 points for both recirculating flow configurations. The values of y+ at the blade wall are lower than 1 in the entire domain.

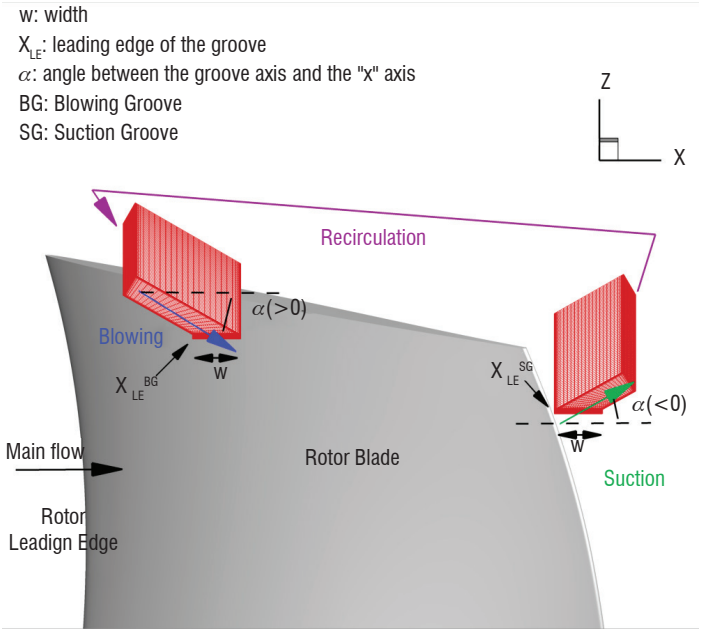


Figure 6 - Schematic set up of the recirculation device (RF1 configuration)

Figure 7 shows the entropy distribution at several axial planes in the main flow path at the nominal operating point. The modification of the topology of the tip leakage vortex is observed. As for the casing treatments, these devices limit the expansion of the tip leakage vortex in the direction perpendicular to the blade chord. Moreover, the entropy is a rational measure of loss in an adiabatic machine [15]. The entropy field shows the significant reduction of the high loss levels with the active control device CB. The losses induced by the tip leakage vortex are lower and the radial and azimuthal extension of the high loss area is smaller. This reduction is increased with the RF2 case. The casing boundary layer thickness and the losses are smaller than the CB ones. The RF2 seems to be the best active control device of this study. The configuration RF1 decreases the casing boundary-layer thickness significantly, but the loss extension is still large, especially in the radial direction.

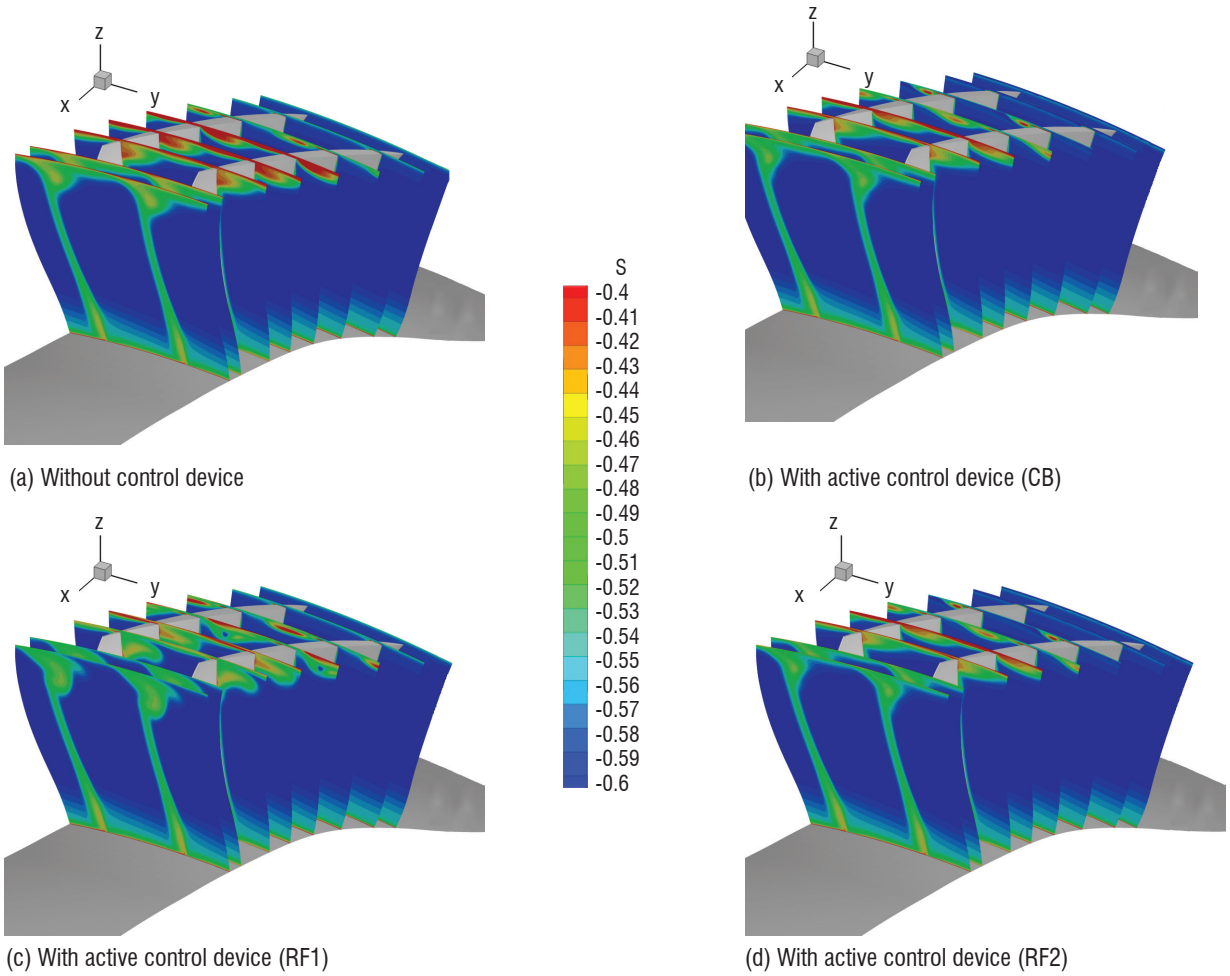


Figure 7 - Entropy field in the main flow path. The blowing and suction grooves are hidden

## Corner and Boundary Layer Flow Control

### Aspirated compressor

#### Experimental investigation

Among flow control techniques investigated to overcome boundary layer separation in highly loaded compressors, Merchant et al. ([32] [33]) and Dang et al. [14] showed that aspiration by boundary layer suction is very promising. In particular, their work has shown that to fully take advantage of aspiration, this flow control technique must be incorporated into the compressor blade design process as early as possible.

Consequently, a 2D direct design method for subsonic aspirated compressor blades was developed at Onera [18]. It provides a simple, fast and reliable means to include aspiration in compressor blade design. It combines a passive separation control with curvature and diffusion, with an active flow control by aspiration ([18][19][20]). One advantage of this approach is to set the aspiration massflow rate necessary to re-attach the flow, quasi-insensitive to inlet Mach number. Continuing the previous developments of this method carried out on a 2D curved diffuser [19] and a 2D subsonic aspirated compressor profile [20], its validation on a test cascade is presented in the following sections [21]. It is intended to show the viability of the aspiration strategy and design criteria as well as the numerical tools and methods employed during the development of this method.

The aspirated cascade blade shown in figure 8-b is built by extrusion of the aspirated blade profile in figure 8-a. The cascade is composed of twelve aspirated blades (marked 1 in figure 8) airtight cantilevered in glass endwalls. With the aid of an auxiliary fan (marked 5 in figure 8), the boundary layer is aspirated by the slot and driven through the blade cavity, then extracted outside of the cascade at each end of the blade (small blue arrows in figure 8-b). All of the blades are connected to aspiration plenums (marked 2 in figure 8) on each side of the cascade. These plenums collect the aspirated air and ensure the same level of aspiration for each blade. Finally, the aspirated air is evacuated from the plenums with pipes towards the aspiration fan. A CAD model of the experiment is presented in figure 8, as well as an enlarged picture of the cascade test section in the *Laboratoire de Mécanique des Fluides et d'Acoustique* at *Ecole Centrale de Lyon* (LMFA).

During the experimental phase of the validation process, the main objective is to determine the performance of the aspirated cascade at mid-span, where the flow surrounding this location approaches 2D conditions. The other objective is to assess the potential of the design method in severe off-design conditions. Thus, the measurements are performed for an inlet flow angle equal to 65°, i.e., at the off-design condition corresponding to +5° of incidence compared to design inlet flow angle of 60°. Particle Image Velocimetry (PIV) is used to measure the velocity in the central blade passage. The PIV set-up is shown in figure 8-d.

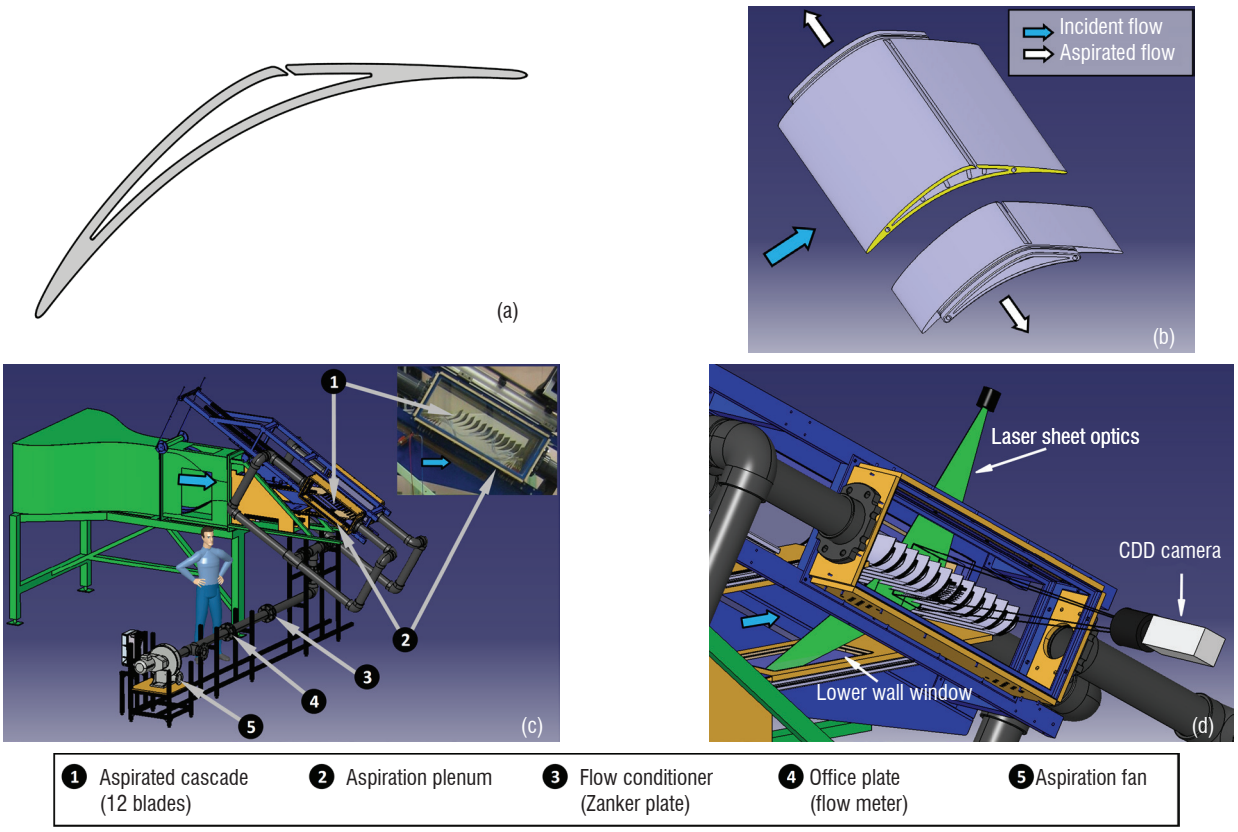


Figure 8 - Aspirated cascade (a) Blade profile (b) Cascade blade (c) Experimental setup (d) PIV setup

The velocity fields, without and with aspiration, measured by PIV in the central blade passage at mid-span are presented in figure 9. They validate capabilities of flow control by aspiration and the relevance of the design method. These results are also remarkable in the sense that they constitute, to the knowledge of the authors, the first PIV measurements of the complete velocity field inside an aspirated cascade. The separated flow without aspiration in figure 9-a, which is induced by a strong variation in blade curvature and diffusion, is reattached with aspiration in figure 9-b. An acceleration of the flow due to aspiration is clearly visible just upstream of the slot in figure 9-b. With the help of the velocity fields in figure 9 in addition to upstream and downstream measurements, the characteristics of the aspirated cascade are calculated. They are summarized in table 3.

| $M_0$ | $M_1$ | $\alpha_0$ | $\alpha_1$ | $C_q$ | $\omega_1$ | $DF$ |
|---|---|---|---|---|---|---|
| 0.123 | 0.0833 | 64.7° | 2.7° | 3.3% | 8.62% | 0.50 |

Table 3 - Experimental characteristics of the aspirated cascade

Table 3 shows that the flow deflection is approximately achieved by the cascade ($\Delta\alpha=62°$), but the aerodynamic loading represented by the Lieblin diffusion factor DF is approximately 60% lower than expected for this flow deflection. This originates from a reduction of the flow diffusion, mainly caused by the presence of massive corner separation invading approximately two thirds of the blade span in total, at the trailing edge. With aspiration, the total pressure loss coefficient $\omega_1$ related to the blade passage reaches 8.62%. This high value comes from the velocity gradient in the pitchwise direction of cascade (visible in figure 9), passed on the total pressure profile downstream of the cascade. Without aspiration, the total pressure loss coefficient reaches 12.58%, which underlines the capacity of aspiration to reduce total pressure losses occurring in the cascade. The velocity field in figure 9-b is obtained with an aspirated mass-flow rate of 3.3%. This value may not be suitable for practical turbomachinery applications since the necessary pressure difference to naturally aspirate this mass flow rate may not be available. However, the aspirated blade profile presented in this paper has not been optimized regarding the aspirated mass flow rate at high incidence angles. Therefore, this value could be improved with blade profile geometry modifications.

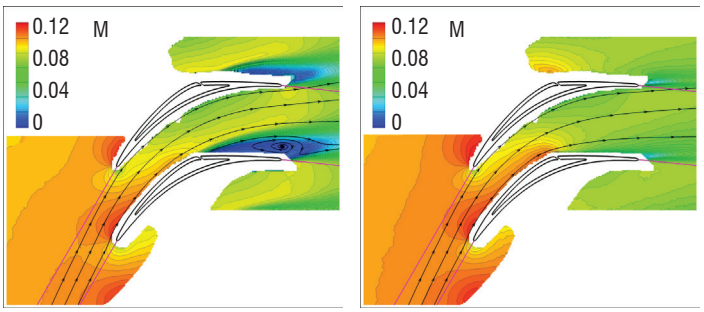


(a) Aspiration off (b) Aspiration On

Figure 9 - Experimental Mach number contours at mid-span

## Numerical investigation

The numerical phase of the validation process aims at reproducing the off-design operation of the experimental aspirated cascade. Due to the significant 3D phenomena observed in the experiment, 3D numerical computations are performed. The numerical simulations of the experimental aspirated cascade used structured grids as shown in figure 10. For an improved aspiration management, the Chimera technique is used to model the technological effect of the shape of the slot and its influence on the main flow.

The structured meshes contain approximately $3.25.10^6$ nodes in total with an average $y^+$ value at the walls equal to 1. Fully-turbulent computations are performed with a Differential Reynolds-Stress Model of turbulence (DRSM). This kind of model is adapted to this case since it takes explicitly into account, without additional modeling, the strong curvature that the streamlines will undergo due to the geometry of the wall, the aspiration and the massive corner separations which are likely to appear. The model used here is the low-Reynolds formulation developed by Speziale et al. [47].

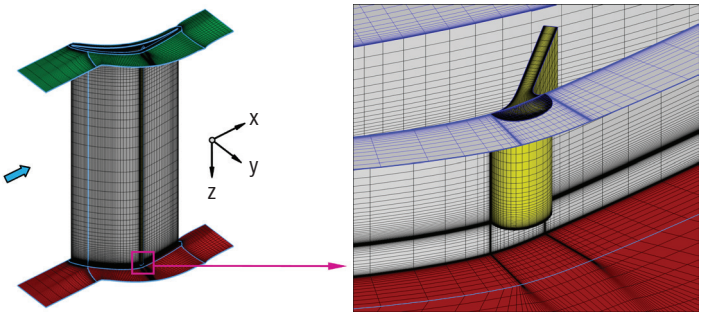


(a) General view (b) Close-up view near an endwall (truncated)

Figure 10 - Computational grids for the simulation of the aspirated cascade experiment.

The comparison between the experimental and numerical results allows assessing the capabilities of CFD in the presence of aspiration and will give further insight on factors influencing the flow behavior with aspiration like the aspiration distribution along the blade span. Due to technical reasons, this feature was not measured during the experiment. Thus, two different aspiration distributions, one uniform (named "3DU") and one non-uniform (named "3DNU") along the spanwise direction are applied and tested in the numerical simulations. They both correspond to an aspiration massflow rate of 3.3%. The non-uniform aspiration distribution profile stems from experimental results obtained on a simplified version of the aspirated blade [18].

The velocity field in the mid-span plane, obtained without aspiration, is presented in figure 11-a. Given the limitations of the RANS approach in simulating separated flow, the general shape and axial extent of the separation is well rendered. However, differences in shape and location of the separation indicate 3D RANS simulations remain qualitative in presence of massive separation.

The 3D RANS simulations perform well with aspiration, as shown in figure 11-b and figure 11-c. Both aspiration configurations "3DNU" and "3DU" are able to reproduce the characteristic features of aspiration described above, namely the flow acceleration upstream of the aspiration slot and the sudden diffusion in the region of the slot. The best agreement with the experimental velocity field is clearly obtained with a uniform aspiration distribution along the blade span. The difference with the non-uniform aspiration distribution is particularly visible in the velocity level upstream of the slot.

The performance of the cascade is summarized in table 4 for both aspirated configurations. In this case, the diffusion factor values at mid-span disclose the difference of the diffusion processes due to the aspiration distribution along the blade span, between the "3DNU" and "3DU" configurations. The higher level of diffusion in the "3DNU" configuration, results in a higher level of the loss coefficient $\omega_1$. However, the computed values are smaller than the experimental ones. The different intensity of the velocity gradient along the pitchwise direction, in the trailing edge region explains such a disparity. Without aspiration, the total pressure loss coefficient calculated from numerical total pressure outlet profiles is equal to 11.19%. The analysis of the previous results shows that the aspiration distribution is also a key aerodynamic feature to take into account for successful design of highly-loaded 3D subsonic aspirated blades.

| | $M_0$ | $M_1$ | $\alpha_0$ | $\alpha_1$ | $C_q$ | $\omega_1$ | $DF$ |
|---|---|---|---|---|---|---|---|
| 3DNU | 0.123 | 0.0670 | 64.7° | 4.0° | 3.3% | 7.69% | 0.63 |
| 3DU | 0.123 | 0.0785 | 64.7° | 3.5° | 3.3% | 7.43% | 0.54 |

Table 4 - Numerical characteristics of the aspirated cascade, with 3DNU and 3DU aspiration distribution

## Vortex Generators

Secondary flow effects like endwall cross-flow or corner separation are responsible for a large part of total pressure losses in a compressor stage. An extensive numerical study of flow control by means of vortex generators applied to the second stage of the CREATE compressor was performed in order to decrease the separation and reduce the losses [38]. The objective of these flow control devices is to produce strong vortices, which enhance mixing between main flow and the decelerated boundary layer at side wall. Different vortex generator geometries and arrangements have been considered on several positions in the compressor flowpath, both at the surface of side walls and on the blades.

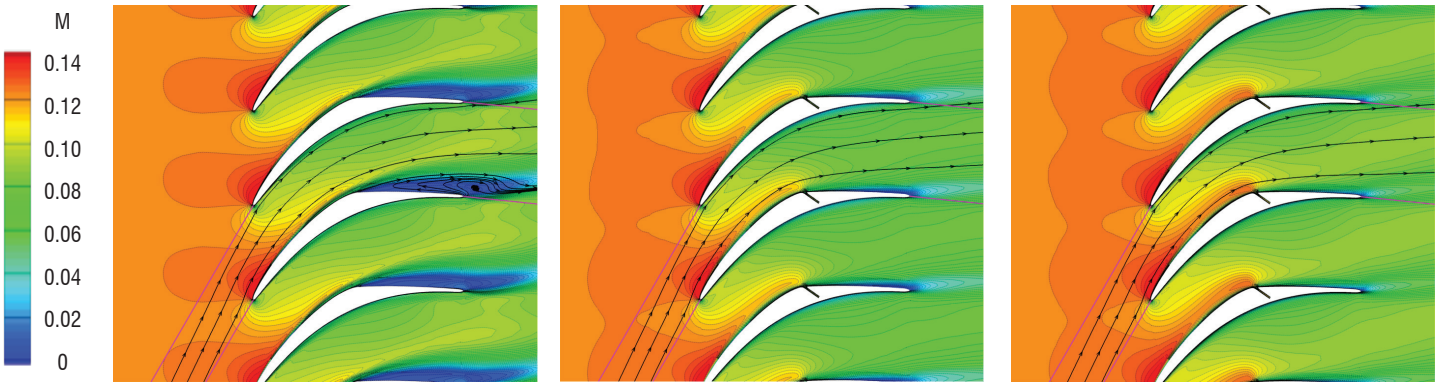


(a) Aspiration off (b) Aspiration on with 3DNU aspiration distribution (c) Aspiration on with 3DU aspiration distribution

Figure 11 - Numerical Mach number contours at mid-span

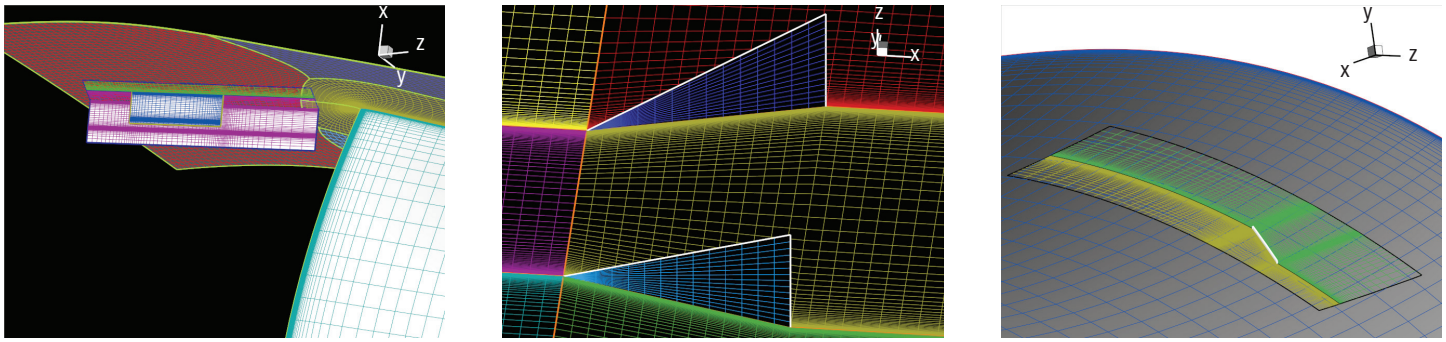


Figure 12 - Details of the overset vortex-generators mesh ahead of the rotor passage (left), mesh for a pair of counter-rotating triangular vortex-generators (center) and for a single rectangular vortex-generator on the blade surface (right)

One critical issue is the way of representing the vortex generators in the Navier-Stokes calculations. Such thought was also made by Chima [11] who developed a body force model to simulate the effects of vortex generators without requiring complicated grids. In the present work, CFD investigations were carried out without using an external body force model but rather by discretizing explicitly the walls of the vortex generator in the CFD grid within the Chimera method.

All computations have been performed under fully turbulent flow assumption, using the $k$-$\varepsilon$ turbulence model. The generation of the VG grids is achieved independently of the surrounding grid for the smooth configuration. A dedicated grid generator has been developed for straight zero-thickness vortex generators with rectangular or triangular planforms. The grid generator enables the automatic discretization of single or several arrangements of vortex, at any position required on the side walls (hub/casing) or on the blade surface (rotor/stator). For each vortex generator, the effects of shape, size, incidence and position as well as mesh extension/refinement parameters are given as input data for the grid generator. The accuracy of the Chimera method then only depends on the mesh definition for the flowpath in which the VG grids are immersed, and its ability to ensure a proper and accurate overlap. A typical representation of the composite mesh for a configuration with one vortex generator per stator passage ahead of a stator vane is shown in figure 12 left.

The vortex generators were sized according to the local boundary layer thickness and blade dimensions. Beside geometrical considerations, the relative position between the vortex generators and the blade and above all the angle of attack relative to the local velocity field are of major importance for the flow control. figure 12 center and right illustrates grids generated for other possible vortex-generators configurations in the framework of the Chimera method. Other possible vortex-generators geometries have been considered within both numerical and experimental investigations ([25][36]).

Both steady and unsteady configurations have been investigated, basically considering fixed rows of vortex generators at the casing ahead of the stator (steady) or ahead the compressor stage (unsteady). Rays of vortex generators distributed radially on the suction side of the stator according to Chima [11] have also been applied for the reduction of the corner stall. Different operating points have been considered. In the two following figures, we show a typical result for an arrangement with 3 VG per blade passage located at the casing ahead of a stator operating at design point. The streamline flow patterns are represented on the stator suction side in the boundary-layer, for the uncontrolled baseline configuration (figure 13 left) and the controlled configuration (figure 13 right). For the baseline configuration, secondary flows in the stator vane passage produce the classical S-shaped flow patterns due to the corner separation: the flowfield entering the blade passage on the suction side is responsible for a cross-passage secondary-flow. For the controlled configuration, the three vortex generators were designed to produce strong counter-rotating vortices relative to the flow direction of the cross passage flow. The dramatic improvement in the flow pattern indicates a large effect on the stator vane flowfield, rising up to nearly half of the blade span at the end of the passage. Actually the secondary flow migration is blocked by the cumulated effects of counter-rotating vortices and the losses are reduced from the mid-height of the blade up to near-wall region. However, in the near-wall region, losses are increased for the controlled case similarly to what has been found and described in [36]. At off-design conditions near stall, a strong flow overturning especially coming from the tip leakage vortex of the previous rotor is responsible for a strong shear-flow in the casing boundary layer. The local velocity flowfield then becomes aligned with the straight vortex generators and vortices are no longer produced. It is anticipated that VG with thickness and camber may be more efficient near stall.

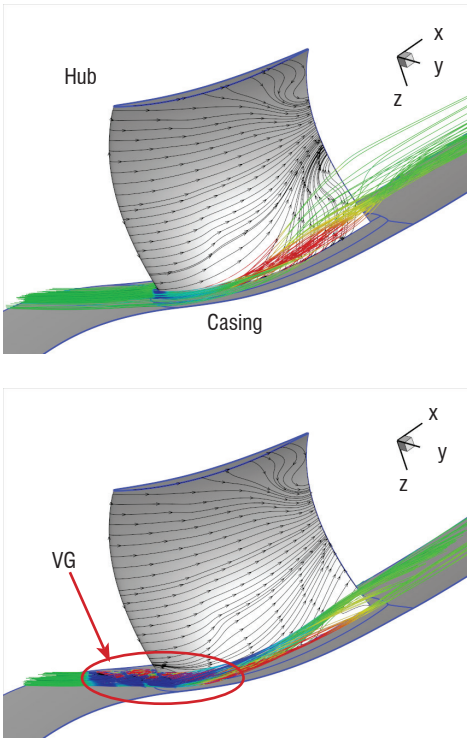


Figure 13 - Corner stall on a stator casing for the baseline stator configuration (left) and reduction of the corner stall for the controlled stator configuration (right)

These preliminary numerical results have shown the ability of vortex generators to reduce secondary flows produced by corner stall in a stator passage at design point. In the vortex-generator design process, it has also been shown that a compromise must be reached between the vortex strength considered to reduce secondary flow phenomena and additional losses associated with the vortex generators and their induced vortex flows.

## Conclusion

This overview of a CFD framework for flow control analysis in turbomachinery applications shows that a wide range of control devices can be modeled and used to improve the efficiency and the operating range of a gas-turbine. The axisymmetrical and non-axisymmetrical slots, injection or recirculating grooves are efficient approaches to extend the stable operating range, especially by increasing the stall margin of a compressor system. The aspirated compressor and vortex generators are also efficient approaches to control the hub corner stall.

The different passive and active control devices are applied to many compressors (CREATE, BUAA, etc.). The integration of several control devices into a single application will be investigated in a future study.

The effectiveness of the control device depends strongly on the smooth configuration. A control device developed on a specific configuration is not directly applicable to another case. A way to overcome this problem is to include the control device design in the global process or within an optimization loop, which will be a further step for improving the design and the effectiveness of control devices for internal flows ■

**Acknowledgements**

The authors wish to thank Snecma (SAFRAN) for its permission to publish this paper.

**References**

[1] D. ARNAUD, X. OTTAVY, A. VOUILLARMET - *Experimental Investigation of the Rotor-Stator Interactions, within a High Speed, Multistage, Axial Compressor. Part 1 - Experimental Facilities and Results*. ASME Turbo Expo 2004, June 14-17, Vienne, Austria, ASME Paper GT2004-53764, 2004.
[2] D. ARNAUD, X. OTTAVY, A. VOUILLARMET - *Experimental Investigation of the Rotor-Stator Interactions, within a High Speed, Multistage, Axial Compressor. Part 2 - Modal Analysis of the Interactions*. ASME Turbo Expo 2004, June 14-17, Vienne, Austria, ASME Paper GT2004-53778, 2004.
[3] J.A. BENEK, J.L. STEGER, F.C. DOUGHERTY - *A Flexible Grid Embedding Technique with Application to the Euler Equations.* AIAA Paper 83-1944, January 1983.
[4] J.A. BENEK, J.L. STEGER, F.C. DOUGHERTY - *A Chimera Grid Scheme.* ASME mini-symposium on advances in grid generation, Houston, 1993.
[5] C. BENOIT, G. JEANFAIVRE, E. CANONNE - *Synthesis of Onera Chimera Method Developed in the Frame of CHANCE Program.* 31st European Rotorcraft Forum, Florence, 2005.
[6] J. BONET, J. PERAIRE - *An Alternating Digital Tree (ADT) Algorithm for 3D Geometric searching and intersection Problems*. International Journal for Numerical Methods in Engineering, Vol. 31, pp-1-17, 1991.
[7] L. CAMBIER, M. GAZAIX - *elsA: an Efficient Object-Oriented Solution to CFD Complexity.* 40th AIAA Aerospace Science Meeting & Exhibit, Reno, USA, 2002.
[8] L. CAMBIER, J.P. VEUILLOT - *Status of the elsA CFD Software for Flow Simulation and Multidisciplinary Applications*. 48th AIAA Aerospace Science Meeting and Exhibit, 2008.
[9] L. CASTILLON, S. PÉRON, C. BENOIT, G. BILLONNET - *Numerical Simulations of Technological Effects Encountered on Turbomachinery Configurations with the Chimera Technique.* 27th International Congress of the Aeronautical Sciences, Nice, France, September 2010
[10] L. CASTILLON, G. LEGRAS - *An Unsteady Overset Grid Method for the Simulation of Compressors with non Circumferential Casing Treatments.* ISABE-2011-1229, Goteborg, Sweden, Sept. 2011.
[11] R.V. CHIMA - *Computational Modeling of Vortex Generators for Turbomachinery*. NASA TM 2002 211551, 2002
[12] E. COLOMBO - *Investigation on the Three-Dimensional Flow Mechanisms in Annular Axial Compressor Cascades for Aero Engines with Flow Control by Aspiration on the Hub and on the Blades*. EPFL PhD Thesis, http://library.epfl.ch/theses/?nr=5241, 2011
[13] A.J. CROOK, E. M. GREITZER, C.S. TAN, J.J. ADAMCZYK - *Numerical Simulation of Compressor Endwall and Casing Treatment Flow Phenomena*. ASME J. Turbomach., 115, pp. 501–512, 1993
[14] T. DANG, M. VAN ROOIJ, L. LAROSILIERE - *Design of Aspirated Compressor Blades Using Three-dimensional Inverse Method*. Proceedings of the ASME Turbo Expo, GT-2003-38492, Atlanta, Georgia, USA, June 16-19, 2003.
[15] J.D. DENTON - *Loss Mechanisms in Turbomachines*. Journal of Turbomachinery, 115:621–656, October 1993.
[16] H. FUJITA, H. TAKATA - *A Study of Configurations of Casing Treatment for Axial Flow Compressors.* Bull. of JSME, Vol. 27, No. 230, pp. 1675-1681, 1985.
[17] S.A. GBADEBO, N.A CUMPSTY, T.P. HYNES - *Control of Three-Dimensional Separations in Axial Compressor by Tailored Boundary Layer Suction*. Journal of Turbomachinery, 130:011004–1–8, January 2008.
[18] A. GODARD - *Etude Numérique et Expérimentale d'un Compresseur Aspiré.* PhD Thesis, Ecole Centrale de Lyon, Lyon, France, 2010.
[19] A. GODARD, S. BURGUBURU and F. LEBOEUF - *Parametric Study of an Aspirated Diffuser.* Proceedings of 7th European Turbomachinery Conference, Athens, Greece, March 5-9, 2007.
[20] A. GODARD, A. FOURMAUX, S. BURGUBURU, F. LEBOEUF - *Design Method of a Subsonic Aspirated Cascade*. Proceedings of the ASME Turbo Expo, GT-2008-50835, Berlin, Germany, June 9-13, 2008.
[21] A. GODARD, F. BARIO, S. BURGUBURU, F. LEBOEUF - *Experimental and Numerical Study of a Subsonic Aspirated Cascade*, Proceedings of the ASME Turbo Expo, GT-2012-69011, Copenhagen, Denmark, June 11-15, 2012.

[22] E.M. GREITZER, J.P. NIKKANEN, D.E. HADDAD, R.S. MAZZAWY, H.D. JOSLYN - *A Fundamental Criterion for the Application of Rotor Casing Treatment.* J. of Fluids Engineering, 101(3), pp. 237–243, 1979.
[23] M.D. HATHAWAY - *Self-Recirculating Casing Treatment Concept for Enhanced Compressor Performance.* ASME TurboExpo, June 3–6, 2002 , Amsterdam, The Netherlands, ASME Paper GT2002-30368, 2002
[24] M.D. HATHAWAY - *Passive Endwall Treatments for Enhancing Stability.* VKI LS 2006-06 on Advances in Axial Compressor Aerodynamics, 2007.
[25] A. HERGT, R. MEYER - *Effects of Vortex Generators Application on The Performance of a Compressor Cascade.* ASME Turbo Expo 2010, GT2010-22464, Glasgow, UK, 2010
[26] G. JEANFAIVRE, C. BENOIT, M.C. LEPAPE - *Improvement of the Robustness of the Chimera Method*, 32nd AIAA Fluid Dynamics Conference, 2002.
[27] G. LEGRAS, N. GOURDAIN, I. TREBINJAC - *Numerical Analysis of the Tip Leakage Flow Field in a Transonic Axial Compressor with Circumferential Casing Treatment.* Journal of Thermal Science, Vol. 19, Issue 3, pp 198-205, June 2010.
[28] G. LEGRAS, L. CASTILLON, N. GOURDAIN, I. TRÉBINJAC - *Flow Mechanisms induced by Non-Axisymetric Casing treatment in a transonic Axial Compressor.* ISAIF10-158, Brussels, Belgium, 4-7 July 2011.
[29] G. LEGRAS, I. TRÉBINJAC, N. GOURDAIN, X. OTTAVY, L. CASTILLON - *A Novel Approach to Evaluate the Benefits of Casing Treatment in Axial Compressors.* International Journal of Rotating Machinery, vol. 2012, Article ID 975407, 19 pages, 2012
[30] F. LIN, F. NING, H. LIU - *Aerodynamics of Compressor Casing Treatment Part I: Experiment and Time-Accurate Numerical Simulation.* ASME Turbo Expo 2008, GT2008-51541, Berlin, Germany, 2008.
[31] R.L. MEAKIN - *Object X-Rays for Cutting Holes in Composite Overset Structured Grids*. AIAA 2001-2537, 2001.
[32] A. MERCHANT - *Design and Analysis of Axial Aspirated Compressor Stages*. PhD Thesis, Massachusetts Institute of Technology, Cambridge, Massachusetts, USA, 1999.
[33] A. MERCHANT, J. KERREBROCK, J. ADAMCZYK, E. BRAUNSCHEIDEL - *Experimental Investigation of a High Pressure Ratio Aspirated Fan Stage.* Journal of Turbomachinery, Vol. 127 (1), pp. 43-51, 2005.
[34] M.W. MÜLLER, H.-P. SCHIFFER, M. VOGES, C. HAH - *Investigation of Passage Flow Features in a Transonic Compressor Rotor with Casing Treatments*. ASME Turbo Expo, Vancouver, British Columbia, Canada, ASME Paper GT2011-45364, June 6-10, 2011.
[35] F. NING, L. XU - *Aerodynamics of Compressor Casing Treatment Part II: A Quasi-Steady Model for Casing Treatment Flows*. ASME Turbo Expo 2008, GT2008-51542, Berlin, Germany, 2008.
[36] J. ORTMANNS, C. PIXBERG, V. GÜMMER - *Numerical Investigation of Vortex Generators to Reduce Cross Passage Flow Phenomena in Compressor Stator Endwalls.* European Turbomachinery Conference 2011, Istanbul, Turkey, Paper ETC9 C075, 2011
[37] R.E. PEACOCK - *Boundary-Layer Suction to Eliminate Corner Separation in Cascades of Aerofoils*. A.R.C. R&M 3663, 1971
[38] A. PESTEIL, D. CELLIER, O. DOMERCQ, V. PERROT, J.C. BONIFACE - *CREATE: Advanced CFD for HPC Performance Improvement.* ASME Turbo Expo 2012. ASME Paper GT2012-68844, Copenhagen, Denmark, 11-15 June 2012
[39] V. PERROT, A. TOUYERAS, G. LUCIEN - *Detailed CFD Analysis of a Grooved Casing Treatment on an Axial Subsonic Compressor*. Proceedings of the 7. European Turbomachinery Conference 2007, March 5-9, Athens, Greece, paper ETC7 016, 2007
[40] D.C. RABE, C. HAH - *Application of casing circumferential grooves for improved stall margin in a transonic axial compressor.* Proceedings of ASME Turbo Expo 2002, Amsterdam, The Netherlands, June 3-6. Paper GT-2002-641, 2002.
[41] A. SACHDEVA - *Analyse, intégration et valorisation des technologies d'aspiration d'aubages dans les compresseurs de turboréacteurs.* PhD Thesis, http://bibli.ec-lyon.fr/exl-doc/TH_T2194_asachdeva.pdf, 2010
[42] TH. SCHWARZ - *Development of a Wall Treatment for Navier-Stokes Computations using overset Grid technique*. Proceedings of the 26th European Rotorcraft Forum, The Hague, September 2000.
[43] G.D.J. SMITH, N. A CUMPSTY - *Flow Phenomena in Compressor Casing Treatment.* ASME Journal of Engineering for Gas Turbines and Power, Vol. 117, pp. 532-541, 1985
[44] Z.S. SPAKOVSZKY, H.J. WEIGL, J.D. PADUANO, C.M. VAN SCHALKWYK, K.L. SUDER, M.M. BRIGHT - *Rotating Stall Control in a High-Speed Stage With Inlet Distortion: Part I - Radial Distortion.* ASME J. Turbomach., 121, pp. 510–516, 1999.
[45] Z.S. SPAKOVSZKY, H.J. WEIGL, J.D. PADUANO, C.M. VAN SCHALKWYK, K.L. SUDER, M.M. BRIGHT - *Rotating Stall Control in a High-Speed Stage with Inlet Distortion: Part II - Circumferential Distortion.* ASME J. Turbomach., 121, pp 517–524, 1999.
[46] P.R. SPALART, S.R. ALLMARAS - *A One-Equation Turbulence Model for Aerodynamic Flows.* La Recherche Aérospatiale, 1:5–21, 1994.
[47] C. SPEZIALE, S. SARKAR, T. GATSKI - *Modelling the Pressure–Strain Correlation of Turbulence: an Invariant Dynamical Systems Approach*. Journal of Fluid Mechanics, 227, pp. 245-272, 2006.
[48] K.L. SUDER, M.D. HATHAWAY, S.A. THORP, A.J. STRAZISAR, M.B. BRIGHT - *Compressor Stability Enhancement Using Discrete Tip Injection.* ASME Journal of Turbomachinery, vol. 123(1), pp. 14-23, 2001
[49] A. TOUYERAS, M. VILLAIN - *Aerodynamic Design and Test Result Analysis of a Three Stage Research Compressor.* ASME Turbo Expo 2004, June 14-17, Vienne, Austria, ASME Paper GT2004-53940, 2004.
[50] H.J. WEIGL, J.D. PADUANO, L.G. FRECHETTE, A.H. EPSTEIN, E.M. GREITZER, M.M. BRIGHT, A.J. STRAZISAR - *Active Stabilization of Rotating Stall and Surge in a Transonic Single Stage Axial Compressor.* ASME J. Turbomach., 120, pp. 625–636, 1998.

## Nomenclature

*Latin*

| | |
|---|---|
| $AVDR$ | Axial velocity density ratio, $AVDR=(1-C_q)\cdot[\rho_1 V_{x1} / \rho_0 V_{x0}]$ |
| $Cp$ | Static pressure coefficient $C_p = (P_{s0} - P_s) / (P_{t0} - P_{s0})$ |
| $Cq$ | Aspirated mass flow rate $C_q = q_f / q_0$ |
| $c$ | Blade chord |
| $DF$ | Lieblein diffusion factor, $DF = 1-(V_1 / V_0) + (\lvert V_{y1} - V_{y0}\rvert / 2\cdot\sigma\cdot V_0)$ |
| $H$ | Blade span |
| $M$ | Mach number |
| $P_t$ | Total pressure |
| $P_s$ | Static pressure |
| $p$ | Blade spacing |
| $q$ | Mass flow |
| $Tu$ | 2D freestream turbulent intensity |
| $V$ | Absolute velocity magnitude |
| $(x,y,z)$ | Cartesian coordinates |

*Greek*

| | |
|---|---|
| $\alpha$ | Absolute flow angle |
| $\beta$ | Yaw angle (pneumatic probe) |
| $\rho$ | Density |
| $\sigma$ | Solidity |
| $\sigma(G)$ | Measurement uncertainty of quantity $G$ |
| $\omega_1$ | Total pressure loss coefficient, regarding the blade passage : $\omega_1 = (1-C_q)\cdot[(P_{t1} - P_{t0}) / (P_{t0} - P_{s0})]$ |

*Subscripts*

| | |
|---|---|
| $0$ | Cascade inlet station |
| $1$ | Cascade outlet station |
| $atm$ | Atmospheric conditions |
| $f$ | Slot outlet station |
| $m$ | Average value |
| $x,y,z$ | Components relative to the x-, y-, z-directions |

## Acronyms

| | |
|---|---|
| 3DNU | (Three-Dimensional Non-Uniform distribution) |
| 3DU | (Three-Dimensional Uniform distribution) |
| BUAA | (Beijing University of Aeronautics and Astronautics) |
| CB | (Casing Blowing) |
| CREATE | (Compresseur de Recherche pour l'Etude des effets Aérodynamiques et TEchnologiques) |
| CT | (Casing Treatment) |
| DRSM | (Differential Reynolds-Stress Model) |
| ECL | (Ecole Centrale de Lyon) |
| HCT | (High Casing Treatment ([34])) |
| LE | (Leading Edge) |
| LMFA | (Laboratoire de Mécanique des Fluides et d'Acoustique) |
| PIV | (Particle Image Velocimetry) |
| RANS | (Reynolds-Averaged Navier-Stokes) |
| RF | (Recirculating Flow configuration) |
| SCT | (Small Casing Treatment ([27])) |
| SW | (Smooth Wall) |
| TE | (Trailing Edge) |
| VG | (Vortex Generator) |

## AUTHORS

**Julien Marty** graduated from Ecole Nationale Supérieure de Mécanique et Aérotechnique (ENSMA) in Poitiers, France. He did a Ph. D thesis in 2010 at Onera Toulouse. He received a Ph. D award from the ISAE-SUPAERO Foundation in December 2011 for his work on the near stall prediction of high pressure compressors. He joined the Applied Aerodynamics Department of ONERA Meudon in 2009 as a research engineer and worked on helicopter rotor optimization using the adjoint method. Since 2011, his main research interests have been the turbulence modeling of separated or vortical flows in compressors and turbines, especially Large-Eddy Simulation and Zonal Detached-Eddy Simulation, transition modeling and the conjugate heat transfer for turbine applications.

**Lionel Castillon** graduated from the Ecole Polytechnique engineering school (Paris) in 1998 and joined Onera in 2000 after a 2 year scholarship at the ENSTA engineering school. He has been working at the Applied Aerodynamic Department on the development and validation of in-house CFD codes for turbomachinery applications.

**Jean-Christophe Boniface** obtained a Master's degree in numerical analysis from the J.-L. Lions laboratory of the University of Paris in 1990, which he completed with a PhD thesis in Computational Fluid Dynamics from the Ecole Nationale Supérieure d'Arts et Métiers (ENSAM, 1995). For 10 years he was involved in CFD code developments at the CFD and Aeroacoustic Department of Onera, especially in the field of rotorcraft flowfield predictions. He then spent 4 years at the University of Milan (Politecnico Di Milano, 2004-2008) as research assistant, working on highly implicit methods and low-speed preconditioning applied to the RANS equations. Since 2008, he joined the Applied Aerodynamics Department of ONERA and is basically working on flow control and optimization for both internal and external aerodynamics.

**Stéphane Burguburu** graduated from the National Institute of Applied Sciences (INSA) in 1995. After a short stay at Onera during his military service, he joined General Electric/Nuevo Pignone as design engineer for centrifugal compressors. After four years, he returned to aerospace as an aerodynamic engineer in the Applied Aerodynamics Department of Onera. He first focused on turbomachinery blade optimization and aeroacoustics, then on the study of the aerodynamics of propellers and open-rotors. Finally, he was the focal point for fans at Onera. He is currently working at Snecma as R&T project leader for low pressure spool aerodynamics and acoustics.

**Antoine Godard** currently holds the position of Research Engineer at the Laboratoire de Mécanique de Fluides et d'Acoustique (LMFA) of the Ecole Centrale de Lyon, France. Prior to this, he was a Research Associate in Compressor Aerodynamics at the Whittle Laboratory of the University of Cambridge, in the United Kingdom. He obtained his doctorate in 2010, in Applied Aerodynamics working at the Office National d'Etudes et de Recherches Aérospatiales (Onera) in cooperation with the Ecole Centrale de Lyon, France. He completed a Master's degree in Mechanical Engineering at the Georgia Institute of Technology in 2004. That same year, he also received his engineering diploma (Diplôme d'ingénieur) from the Ecole Nationale Supérieure d'Arts et Métiers (ENSAM). His current research interests are flow-controlled compressor design, separated flow patterns, compressor aerodynamic stability, experimentation and design of experimental facilities.